Fields in Planar Anisotropic Transmission-Line Metamaterials

Joshua K. H. Wong, *Student Member, IEEE*, Keith G. Balmain, *Life Fellow, IEEE*, and George V. Eleftheriades, *Fellow, IEEE*

***Abstract*—An electromagnetic analysis of wave propagation in planar anisotropic transmission-line metamaterials is presented. It is shown that a planar square-celled grid, series-loaded with orthogonal inductors and capacitors and positioned over a ground plane, is magnetically anisotropic and may be described in terms of a diagonal permeability tensor. Resonance cone field concentrations form when two of the three diagonal elements of the permeability tensor are opposite in sign and the dispersion surface becomes hyperbolic. A theoretical treatment of an electric line current source excitation shows that the formation of resonance cones is a consequence of the singularity associated with the characteristic surface of a hyperbolic equation. The resonance cone angle, which also describes the direction of local power flow in the region between the grid and the ground plane, can be predicted to a good degree of accuracy. To the authors' best knowledge, the present work also verifies experimentally for the first time that current flow reverses direction across the resonance cone. Experiments, simulations, and analytical calculations of the cone angle are in good agreement.**

***Index Terms*—Anisotropic metamaterials, counter-flowing cone currents, hyperbolic dispersion surface, resonance cone.**

I. Introduction

THE objective of this work is to provide a comprehensive study of wave propagation in planar anisotropic transmission-line metamaterials including theory, numerical computations and experiments. The present work follows directly from [1] and has its root in the quasi-static theory of antennas in uniaxial anisotropic plasmas. In that context, resonance cones emerge as conical high-field regions that extend outward from the antenna extremities under the condition that two of the three diagonal elements of the plasma permittivity tensor are opposite in sign. These conical high-field regions have an axis that is parallel to the static magnetic field and an opening angle that varies with the incident frequency, the plasma density, and the static magnetic field strength. In 1969, Fisher and Gould performed the first measurements on these high-field regions and were also the first to call them resonance cones [2].

Later in the same year, Balmain and Oksiutik [3] noted that the negative and positive permittivities could be interpreted by representing the medium in terms of arrays of inductors and capacitors respectively. Following from this idea, Balmain *et al.* [4] demonstrated experimentally for the first time that resonance cones could exist when a planar square-celled wire grid is loaded with inductors and capacitors. Furthermore, Balmain *et al.* [4] pointed out that if one adopts the somewhat oversimplified viewpoint of circuit theory, one finds that the resonance cone directions are simply the directions of the point-to-point zeros in reactance measured across the grid surface.

Mathematically speaking, resonance cones are just the conical characteristic surfaces associated with a hyperbolic partial differential equation, those surfaces being the surfaces along which discontinuities propagate. Thus, as pointed out in [5], an anisotropic plasma excited by a point source at a single frequency would exhibit resonance cones since the partial differential equation for the scalar potential is hyperbolic in the space coordinates. Of course, this is not confined to electrostatics but it is also true in the magnetostatic limit, where the partial differential equation for the scalar magnetic potential is also hyperbolic in the space coordinates [6]. Therefore we should not be surprised to find that resonance cones also exist in magnetized ferrites [7] where two of the three diagonal elements of the ferrite permeability tensor are opposite in sign. Indeed, it will be shown further on in this paper, that a planar wire grid positioned over ground and loaded with arrays of inductors and capacitors is magnetically anisotropic and possesses a diagonal permeability tensor where two of the three diagonal permeabilities have opposite signs. In other words, propagation in the wire grid is governed by a hyperbolic differential equation and supports the formation of resonance cones. This notion of describing the metamaterial presented in [4] in terms of of a magnetically anisotropic medium is compatible with the analysis presented in [8]. For the sake of completeness, we should mention that the resonance cone phenomenon is also observed in unloaded transmission-line grids [9] by utilizing phase cancellation along a prescribed propagation direction. However, in that context, an effective permeability cannot be defined since the unit cells are comparable in size to the operational wavelength. Thus, although the unloaded transmission-line grids exhibit resonance cone phenomena, they differ fundamentally from the structure presented here where the unit cells are much smaller than a wavelength.

The metamaterial configuration of interest here is based on [4] and is shown in Fig. 1. It consists of a two-dimensional wire grid series-loaded with orthogonal capacitors and inductors and positioned over a ground plane. The existing literature on this metamaterial focuses on numerical simulations and experimental results [1], [4], [8]. However, there are no theoretical treatments on subjects such as how the metamaterial is modeled, how waves propagate within the metamaterial, or how the power flows when

Manuscript received July 18, 2005; revised April 20, 2006. This work was supported in part by Defence Research and Development Canada (Ottawa), and in part by the Natural Sciences and Engineering Research Council of Canada.

The authors are with The Edward S. Rogers Sr. Department of Electrical and Computer Engineering, University of Toronto, Toronto, ON M5S 3G4, Canada (e-mail: joshua@waves.utoronto.ca).

Digital Object Identifier 10.1109/TAP.2006.882158

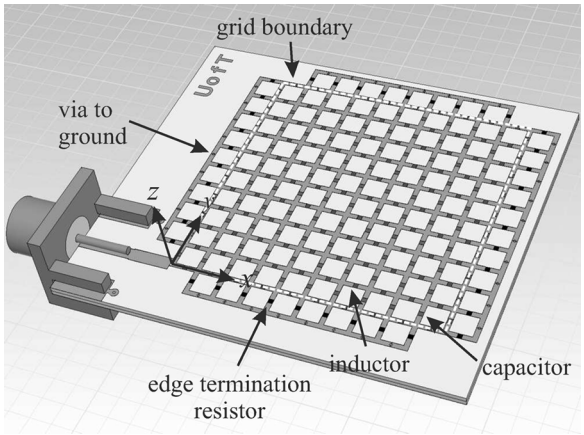

Fig. 1. Simulation model of the uniform anisotropic transmission-line metamaterial over ground with corner feed and resistive edge-loading. The inductors are in parallel to the x-axis and the capacitors are in parallel to the y-axis. The grid boundary is denoted by the white dashed line.

excited by a source. In this paper, we build on the viewpoint of circuit theory presented in [4] and develop an electromagnetic analysis of wave propagation in planar anisotropic transmission-line metamaterials based on a quasi-TEM approximation. By quasi-TEM, we mean that the longitudinal fields of the propagating wave are assumed to be negligible [10]. We use the quasi-TEM approximation to develop the material parameters and show that the metamaterial can be described by a diagonal permeability tensor. We show theoretically, and verify through experiments, that the quasi-TEM approximation provides an accurate description of the fields inside the presented metamaterial. Following this assumption, we confirm experimentally that the resonance cone angle can be predicted analytically to a good degree of accuracy. Furthermore, we show theoretically how the power flows in an equivalent, continuous metamaterial when excited by an infinite filamentary electric line current source. Finally, we report for the first time the experimental observation of the counter-flowing current distribution across a resonance cone. This type of current distribution was first found in a quasi-static analysis of an electrically anisotropic homogeneous medium excited by a long filament of magnetic current [11].

II. Effective Permeability Tensor

We begin our analysis by determining the effective permeability tensor. This enables us to find the condition under which two of the three diagonal elements are opposite in sign. Consider Maxwell's equations for a propagating wave along a microstrip line

$$\nabla \times \mathbf{E} = -\frac{\partial \mathbf{B}}{\partial t} \tag{1a}$$

$$\nabla \times \mathbf{H} = \frac{\partial \mathbf{D}}{\partial t}. \tag{1b}$$

For a diagonal permeability tensor $\boldsymbol{\mu}$ and a scalar permittivity ε, (1) can be written in terms of Cartesian components as

$$\frac{\partial E_z}{\partial y} - \frac{\partial E_y}{\partial z} = -\mu_x \frac{\partial H_x}{\partial t} \tag{2a}$$

$$\frac{\partial E_x}{\partial z} - \frac{\partial E_z}{\partial x} = -\mu_y \frac{\partial H_y}{\partial t} \tag{2b}$$

$$\frac{\partial E_y}{\partial x} - \frac{\partial E_x}{\partial y} = -\mu_z \frac{\partial H_z}{\partial t} \tag{2c}$$

and

$$\frac{\partial H_z}{\partial y} - \frac{\partial H_y}{\partial z} = \varepsilon \frac{\partial E_x}{\partial t} \tag{3a}$$

$$\frac{\partial H_x}{\partial z} - \frac{\partial H_z}{\partial x} = \varepsilon \frac{\partial E_y}{\partial t} \tag{3b}$$

$$\frac{\partial H_y}{\partial x} - \frac{\partial H_x}{\partial y} = \varepsilon \frac{\partial E_z}{\partial t}. \tag{3c}$$

For propagation along the x direction, the non-zero field components are E_z and H_y since in the context of a quasi-TEM analysis, propagation in a microstrip line is similar to propagation in a parallel-plate waveguide where the longitudinal fields are negligible and E_z dominates over E_y. Thus, (2) and (3) reduce to

$$\frac{\partial E_z}{\partial x} = \mu_y \frac{\partial H_y}{\partial t} \tag{4a}$$

$$\frac{\partial H_y}{\partial x} = \varepsilon \frac{\partial E_z}{\partial t}. \tag{4b}$$

On the elimination of H_y, we get

$$\frac{\partial^2 E_z}{\partial x^2} = \mu_y \varepsilon \frac{\partial^2 E_z}{\partial t^2}. \tag{5}$$

The voltage $V(x)$ between the microstrip and the ground can be found by integrating (5) along the height of the substrate. In the time-harmonic steady-state condition, the integration gives

$$\frac{d^2 V(x)}{dx^2} + \omega^2 \mu_y \varepsilon V(x) = 0. \tag{6}$$

Now, the Telegrapher's equations of a transmission line with distributed inductance L_x (H/m) and capacitance C_z (F/m) are given by

$$\frac{dV(x)}{dx} = -j\omega L_x I(x) \tag{7a}$$

$$\frac{dI(x)}{dx} = -j\omega C_z V(x) \tag{7b}$$

On the elimination of $I(x)$, we obtain the second-order differential equation for the voltage along the transmission line and get

$$\frac{d^2 V(x)}{dx^2} + \omega^2 L_x C_z V(x) = 0. \tag{8}$$

Comparing (4) with (7) as well as (6) with (8), we can establish the equivalences

$$\mu_y = L_x \tag{9}$$

$$\varepsilon = C_z. \tag{10}$$

Applying the same procedure to propagation in the y direction, we get

$$\mu_x = L_y \tag{11}$$

$$\varepsilon = C_z. \tag{12}$$

Now, if the transmission line of length d is loaded with a series impedance Z_s, the effective per unit length inductance becomes

$$L_{effx,effy} = L_{x,y} - j\frac{Z_s}{\omega d}. \tag{13}$$

Therefore, the impedance is $Z_s = j\omega L$ for a line loaded with a series inductor and $Z_s = 1/j\omega C$ for a line loaded with a series capacitor. In this way, we can describe the metamaterial shown in Fig. 1 by the effective permeability tensor

$$\boldsymbol{\mu} = \begin{pmatrix} \mu_x & 0 & 0 \\ 0 & \mu_y & 0 \\ 0 & 0 & \mu_z \end{pmatrix} \tag{14}$$

where

$$\mu_x = L_y - \frac{1}{\omega^2 C d} \tag{15a}$$

$$\mu_y = L_x + \frac{L}{d} \tag{15b}$$

$$\mu_z = \mu_0. \tag{15c}$$

For the metamaterial of interest, $L_x = L_y$ since the interconnecting transmission lines have the same properties.

From (15), we see that μ_y and μ_z are always positive. Therefore, resonance cones can form only when μ_x is negative. From (15a) this occurs in the frequency range

$$\omega < \frac{1}{\sqrt{L_y C d}}. \tag{16}$$

III. Propagation Characteristics

Once the permeability tensor is thus determined, we can proceed to deal with the effects of anisotropy in the metamaterial. To understand electromagnetic propagation in the metamaterial whose characteristics are a function of the propagation direction, it is useful to treat the metamaterial as a uniform homogeneous anisotropic medium.

Considering time-harmonic fields in a source-free region with scalar permittivity ε and dyadic permeability $\boldsymbol{\mu}$, we can write the Helmholtz equation for the magnetic field as

$$\mathbf{k} \times (\mathbf{k} \times \mathbf{H}) + \omega^2 \varepsilon \boldsymbol{\mu} \cdot \mathbf{H} = 0. \tag{17}$$

Substituting (14) into (17) and considering propagation in the xy-plane, we obtain the dispersion equation

$$\frac{k_x^2}{\mu_y} + \frac{k_y^2}{\mu_x} = \omega^2 \varepsilon. \tag{18}$$

In the frequency range where μ_x is negative, the dispersion equation becomes hyperbolic. Fig. 2 shows the dispersion surface of the metamaterial from 1.0 to 2.0 GHz with $L = 3.6$ nH and $C = 2.7$ pF. Contour projections of the dispersion surface at 1.0 and 2.0 GHz are projected at the bottom of the graph which shows the hyperbolic characteristics of the dispersion relation. Furthermore, we can observe that plane-wave propagation is confined spatially to the regions $\varphi < \theta$. For $\varphi > \theta$, the wave number is imaginary and propagation is evanescent. This region is sometimes known as the "shadow region" in plasma science [12]. The group velocity vector $\mathbf{v}_g$ and the Poynting vector $\mathbf{S}$, however, are confined to the interior of the conical

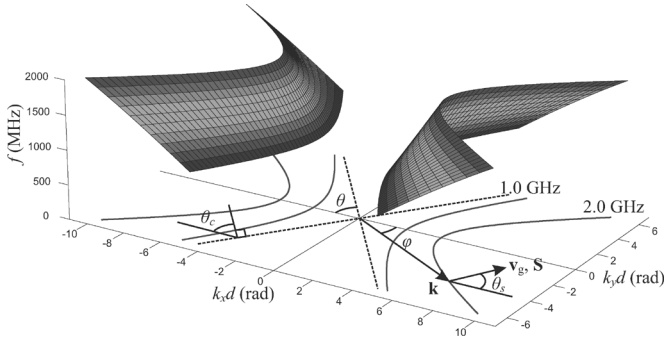

Fig. 2. Dispersion surface of the metamaterial from 1.0 to 2.0 GHz. Constant frequency contours at 1.0 and 2.0 GHz are projected at the bottom of the graph. The asymptotes for the 1.0 GHz surface are shown by the dashed lines. The angle between the asymptote and the $k_x d$ axis is denoted by θ.

regions $|\tan\theta_s| < \tan\theta_c$. The limiting angle θ_c for the group velocity vector is defined by the perpendicular to the asymptote of the dispersion surface in Fig. 2 and can be evaluated from (18) as

$$\tan\theta_c = \sqrt{\left|\frac{\mu_y}{\mu_x}\right|} \tag{19}$$

which is the complementary angle of the limiting angle θ for the wavevector. Thus, plane-wave propagation for $\mu_x < 0$ is confined to certain regions in space and, as we will show in the next section, if the medium is excited by a line source, the energy is concentrated along the characteristic surface associated with the hyperbolic dispersion equation.

IV. Power Flow Due to an Infinite, Filamentary, Electric Line Current Source

Our discussion in the previous section emphasized a qualitative interpretation of the field behavior which so far has ignored the presence of excitations. In this section, we continue our analysis and investigate radiation problems in a uniform homogeneous anisotropic medium whose permeability tensor is given by (14). We consider an infinite, filamentary, electric line current source $\mathbf{J}$ oriented parallel to the z-axis and given by

$$\mathbf{J} = I_0 \delta(x)\delta(y)\hat{\mathbf{z}}. \tag{20}$$

Since the electric line current source extends to infinity in the z-direction with a zero z derivative, the non-vanishing fields for propagation transverse to the z-axis are E_z, H_x, and H_y. As a result, the magnetic fields can be written as

$$H_x = -\frac{1}{j\omega\mu_x}\frac{\partial E_z}{\partial y} \tag{21a}$$

$$H_y = \frac{1}{j\omega\mu_y}\frac{\partial E_z}{\partial x}. \tag{21b}$$

Introducing the anisotropy factor $a^2 = \mu_x/\mu_y$ and defining $\beta_y^2 = \omega^2\mu_y\epsilon$, we can see that the inhomogeneous wave equation for the electric field becomes

$$\left(\frac{\partial^2}{\partial x^2} + \frac{1}{a^2}\frac{\partial^2}{\partial y^2} + \beta_y^2\right) E_z = j\omega\mu_y I_0 \delta(x)\delta(y). \tag{22}$$

To solve for the fields, we employ a scaling procedure [13] and scale equation (22) to reduce the differential operator in the

xyz coordinates into a Laplacian operator in the $x\eta z$ coordinates. Using the scaling factor $\eta = ay$ and writing the electric field as

$$E_z(x,\eta) = j\omega\mu_y a I_0 G(x,\eta) \tag{23}$$

we can write (22) in the $x\eta z$ coordinates as

$$\left(\frac{\partial^2}{\partial x^2} + \frac{\partial^2}{\partial \eta^2} + \beta_y^2\right) G(x,\eta) = \delta(x)\delta(\eta). \tag{24}$$

Thus the solution to (24) is

$$G(x,\eta) = \frac{j}{4} H_0^{(2)}(\beta_y \sqrt{x^2+\eta^2}). \tag{25}$$

To calculate the field components, we substitute (25) into (23) and then scale back into the xyz coordinates. Thus, the electric field becomes

$$E_z = -\frac{\omega}{4}\mu_y a I_0 H_0^{(2)}(\beta_y \sqrt{x^2+a^2y^2}) \tag{26}$$

and the magnetic fields can be found by substituting (26) into (21a) and (21b). Therefore, we have

$$H_x = \frac{j}{4} a\beta_y I_0 H_1^{(2)}(\beta_y \rho\nu(\varphi)) \frac{\sin\varphi}{\nu(\varphi)} \tag{27a}$$

$$H_y = -\frac{j}{4} a\beta_y I_0 H_1^{(2)}(\beta_y \rho\nu(\varphi)) \frac{\cos\varphi}{\nu(\varphi)}. \tag{27b}$$

where $\rho\nu(\varphi) = \sqrt{x^2+a^2y^2}$. In cylindrical coordinates, (27a) and (27b) can be combined to yield the magnetic field components as

$$\begin{aligned} H_\rho &= H_x\cos\varphi + H_y\sin\varphi \\ &= 0 \end{aligned} \tag{28a}$$

$$\begin{aligned} H_\varphi &= -H_x\sin\varphi + H_y\cos\varphi \\ &= -j\frac{a\beta_y I_0}{4\nu(\varphi)} H_1^{(2)}(\beta_y\rho\nu(\varphi)). \end{aligned} \tag{28b}$$

Since we are interested in the far-field behavior where ρ is large, we can apply the large-argument approximation of the Hankel functions [14]

$$\lim_{x\to\infty} H_v^{(2)}(x) = \sqrt{\frac{2j}{\pi x}} j^v e^{-jx} \tag{29}$$

and calculate the time-average radiated power density. As a result, we get

$$\begin{aligned} S_\rho &= \frac{1}{2}\mathrm{Re}\left(-E_z H_\varphi^*\right) \\ &= \begin{cases} \frac{\omega I_0^2}{16\pi\rho}\frac{\mu_y a^2}{\nu^2(\varphi)} & \nu(\varphi) \text{ is real} \\ 0, & \nu(\varphi) \text{ is imaginary} \end{cases} \end{aligned} \tag{30a}$$

$$S_\varphi = 0 \tag{30b}$$

$$S_z = 0. \tag{30c}$$

Thus, no energy penetrates into the shadow region when the propagation direction is greater than the limiting angle of the wavevector since $\nu(\varphi)$ is imaginary.

If we rewrite the non-zero part of (30a) as

$$S_\rho = \frac{\omega I_0^2}{16\pi\rho}\left(\frac{\mu_x\mu_y}{\mu_y\cos^2\varphi + \mu_x\sin^2\varphi}\right) \tag{31}$$

we can see that the power density contains a singularity when

$$\mu_y\cos^2\varphi + \mu_x\sin^2\varphi = 0. \tag{32}$$

Rearranging (32), we get

$$\tan\varphi = \sqrt{\left|\frac{\mu_y}{\mu_x}\right|} \tag{33}$$

which is exactly the limiting angle for the group velocity vector shown in (19). Looking at (30), we can see that the singularity causes the power to concentrate along the direction of θ_c. Furthermore, the singularity renders the total radiated power infinite, an anomaly that is known as the "infinity catastrophe" [15]. The singularity is a result of the lossless material model and methods to remove it were investigated extensively by Felsen [16] and Balmain [5]. Equations (26), (28a), and (28b) illustrate an important point that arises when the dispersion equation of the metamaterial contains an open branch—the fields diverge on the shadow boundary, which is just the characteristic surface at which resonance cones exist [5].

The formulation of the fields in terms of the Green's function was obtained from Maxwell's equations in cylindrical coordinates subject to the constraint $\partial/\partial z = 0$. Thus, the interpretation of these results follows also from the dispersion surface. Since the fields are independent of z, the relevant portions of the dispersion surface are the curves obtained by intersection with the $k_z = 0$ plane, which are the same curves shown in Fig. 2. Finally, we should mention that the same result could be obtained directly by applying duality to the solution presented in [12], where Felsen solved the problem of radiation due to a magnetic line current embedded in an anisotropic plasma half-space.

V. Full-Wave Simulations

We employ Ansoft's HFSS to investigate wave propagation in the metamaterial and whether the quasi-TEM analysis is an appropriate approximation. Simulations provide a means to study the field distribution inside the metamaterial at points not accessible with experiments. The present paper expands upon the previous works in part by examining the simulated magnetic fields within the substrate.

For the representation of the metamaterial shown in Fig. 1, the lumped components were modeled as zero-thickness finite-impedance strips joining lengths of finite-thickness microstrip lines. The simulation model is composed of a wire grid realized on a 31 mil thick Rogers RO4003C substrate and has 10 by 10 cells, each cell 2.0 mm square. The edges of the grid are terminated with 50 Ω resistors and are connected to the ground plane by vias with a diameter of 200 μm. The interconnecting transmission lines are 16 μm thick and have a characteristic impedance of 100 Ω. The substrate dielectric constant is 3.38. The series-loaded inductance and capacitance are 3.6 nH and 2.7 pF respectively.

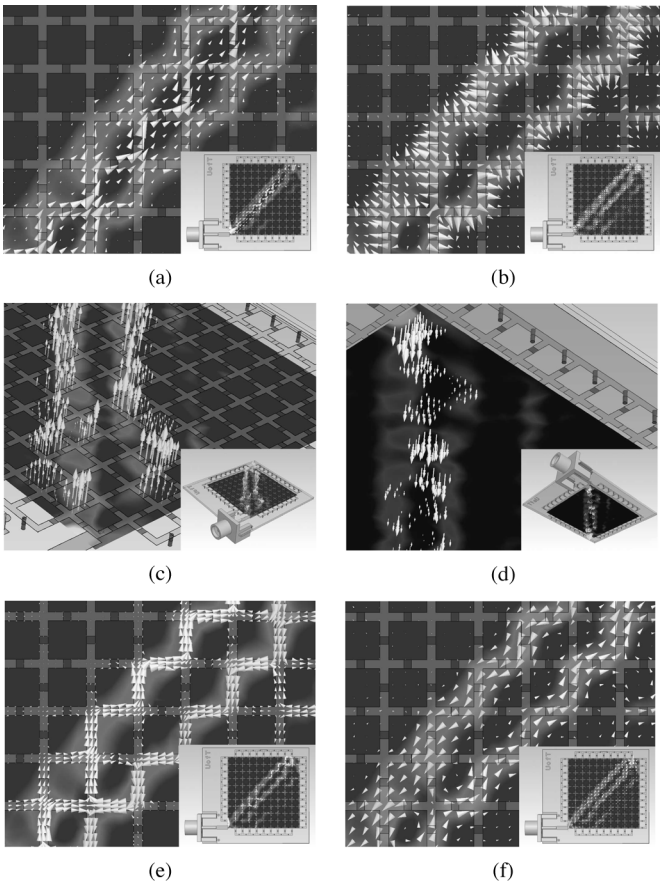

Fig. 3. Simulated field plots showing the field distributions and the current density in the metamaterial at 1.47 GHz. The lightly shaded region shows the location where the current density is highest. The size of the arrow head is proportional to the field strength. The insets show the orientation of the board with respect to the view angle. (a) Poynting vector real part; (b) horizontal magnetic field ($\mathbf{H}_{xy}$); (c) positive vertical magnetic field ($\mathbf{H}_z > 0$); (d) negative vertical magnetic field ($\mathbf{H}_z < 0$); (e) vector current density ($\mathbf{J}$) in the grid plane; (f) vector current density ($\mathbf{J}$) in the ground plane.

The field distributions within the metamaterial are shown in Fig. 3, which displays the Poynting vector real part, the magnetic fields and the vector current densities at the grid and on the ground plane. The simulation was performed at 1.47 GHz. For each graph, the scalar magnitude of the current density is superimposed on the ground plane. The lightly shaded region depicts the path of the resonance cone. Fig. 3(a) shows the Poynting vector real part calculated in the middle of the substrate. It can be seen that power flow is directed along the resonance cone. Fig. 3(b) to (d) show the magnetic field distributions computed in the middle of the substrate. We can see from Fig. 3(b) that the horizontal components of the magnetic fields are transverse to the microstrip lines along the resonance cone. Furthermore, the vertical components of the magnetic field real part, as shown in Fig. 3(c) and Fig. 3(d), show that the current flow reverses direction across the resonance cone, which is also seen in an anisotropic grid both with and without a ground plane [11]. To confirm this hypothesis of counter-flowing currents across the resonance cone, we plot the vector current density calculated at the grid and the ground plane as shown in Fig. 3(e) and Fig. 3(f). Furthermore, by comparing Fig. 3(e) and (f), we can see that the current also flows in opposite directions on the grid and the ground plane, which is characteristic of a propagating TEM wave in a parallel-plate waveguide and confirms the validity of the quasi-TEM analysis.

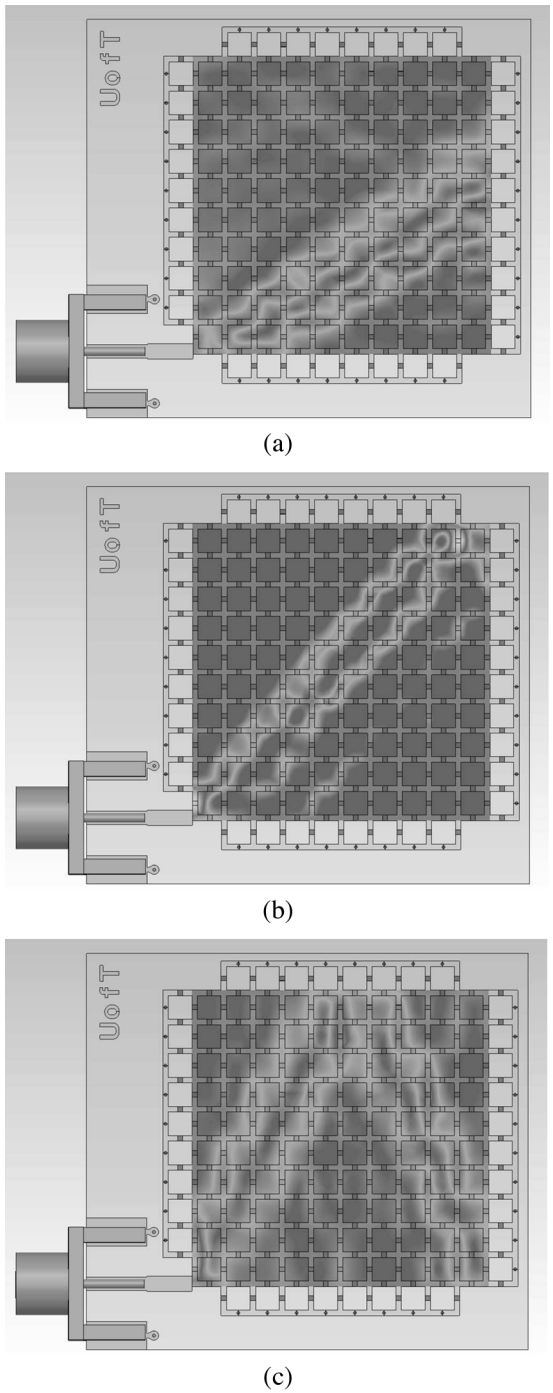

Fig. 4. Plots showing the simulated current density magnitude on the ground plane at three frequencies. (a) 1.00 GHz; (b) 1.47 GHz; (c) 2.00 GHz.

To study power flow in the metamaterial, we make use of the simulated scalar magnitude of the current density which is shown in Fig. 4 for various frequencies. Since the refractive index is an implicit function of frequency, we expect the direction of the resonance cone, or power flow for that matter, to change with frequency. The plot shows the way the resonance cone orientation scans with frequency over the three frequencies employed. As the frequency is increased, the cone angle

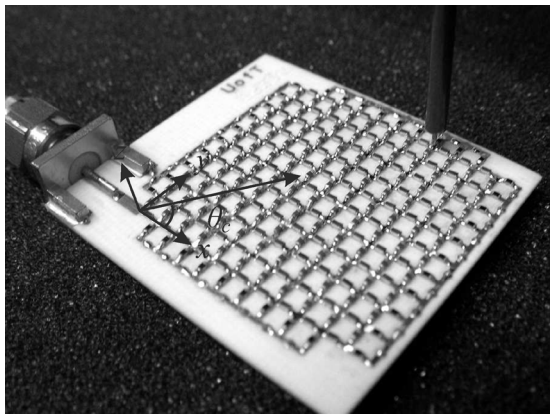

Fig. 5. Experimental setup showing the near-field scanning probe.

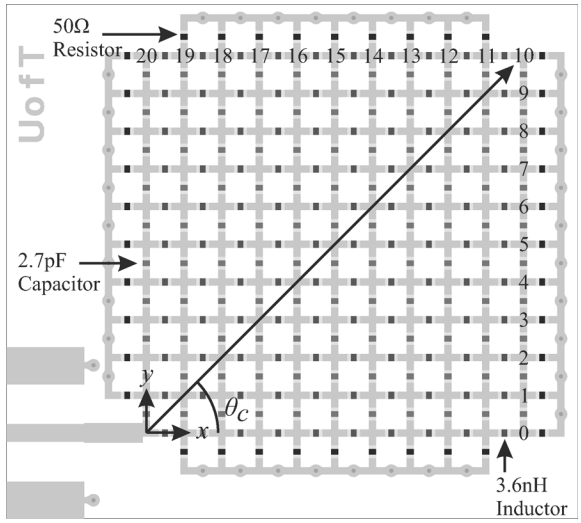

Fig. 6. Schematic view of the metamaterial used in the experiment. Also shown in the drawing are the measurement points labeled with numbers.

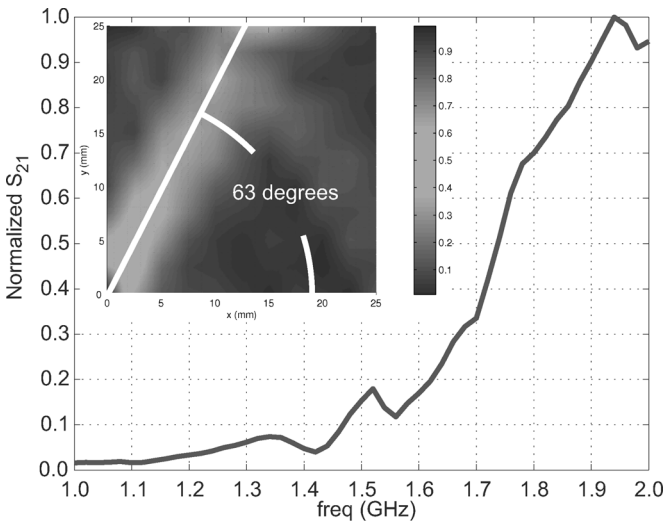

Fig. 7. Normalized forward transmission magnitude measured at node 15 showing a peak at 1.94 GHz which has a corresponding resonance cone angle of 63°. The inset shows the normalized S_{21} magnitude measured across the surface of the grid at 1.94 GHz.

θ_c increases. This is in agreement with (19), since μ_x decreases with increasing frequency. In Fig. 4(c), specular reflection from the grid edge is visible and is most likely due to impedance mismatch. Also visible are the two streams of current which is characteristic of the counter-flowing currents mentioned in the foregoing paragraph.

VI. Experimental Results and Measurement Technique

We conclude our study by performing resonance cone angle measurements. The experimental setup is shown in Fig. 5. The transmit port of the network analyzer is connected to the SMA connector and the receive port is connected to the near-field scanning probe (open-ended coaxial cable). In the experiment, the vertical E-field is picked up by the near-field scanning probe and the S_{21} is measured which, when plotted on a linear scale, is approximately proportional to the grid-to-ground voltage.

A straightforward but time consuming approach to measure the cone angle is to fix the frequency on the network analyzer and measure the forward transmission magnitude (S_{21}) at each node along the edges of the grid as shown in Fig. 6. Thus, the cone angle is simply the angle θ_c between the x-axis and the line connecting the origin to the node with the largest S_{21} magnitude as shown in Fig. 6. In this way, the frequency becomes the independent variable and the cone angle is the dependent variable. However, using this method would require us to probe 19 points for each frequency. Depending on the frequency resolution of the network analyzer, this would amount to a large number of measurements. For example, a frequency resolution of 501 points over the frequency range of interest means that we must perform over 10,000 measurements.

Alternatively, we can let the cone angle be the independent variable and measure the frequency at which the S_{21} magnitude is largest. In fact, this is how Fisher and Gould [17] performed their resonance cone angle measurements in anisotropic plasma in their pioneering contributions to the study of resonance cone phenomena. In this case, the near-field probe would scan along the edges of the grid from node 1 to node 20, and at each node a frequency-swept S_{21} measurement would be made. Doing so allows us to determine the frequency at which the S_{21} magnitude is largest. As a representative example, consider the normalized S_{21} magnitude response measured at node 15 as shown in Fig. 7. We can see from the plot that the peak magnitude occurs at 1.94 GHz. Since the line joining the origin to node 15 makes an angle of 63° with the x-axis, we can therefore say that the cone angle at 1.94 GHz is 63°. A plot of the experimentally observed cone angle versus frequency is shown in Fig. 8. On the same graph, the cone-angle-frequency relationship predicted by (19) and simulation are plotted. The theory and experiment are in good agreement except in the extreme cases where the resonance cone is in close proximity to the edge of the grid. The discrepancies can be seen near the band edges in Fig. 8. Near the band edges, the resonance cone is almost parallel to one of the grid edges. Since the grid edges are terminated with low impedance to minimize reflections, this steers the current associated with the resonance cone to flow toward the grid edge and as a result, distorts the measured resonance cone angle from what is predicted by the theory.

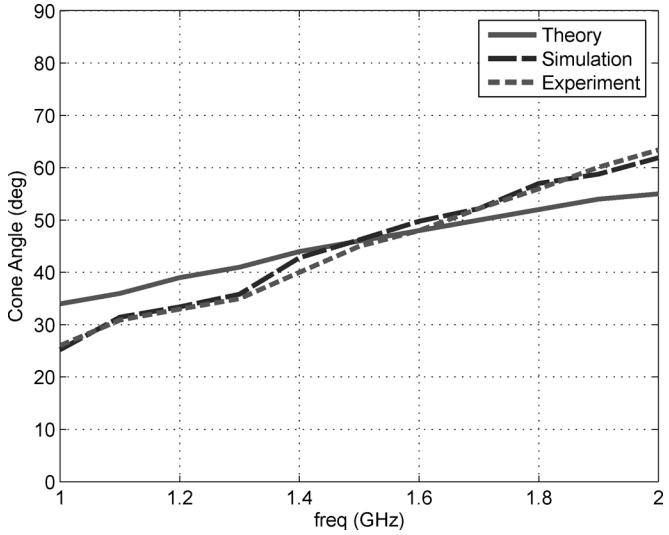

Fig. 8. Graph showing the experimentally observed resonance cone angle versus frequency relationship. The solid curve is the one predicted by (19).

VII. Experimental Verification of Counter-Flowing Currents

In the full-wave simulations presented earlier, we had discussed the notion of currents flowing in opposite directions across the resonance cone. To verify this concept, we make use of the S_{21} magnitude and phase responses at two adjacent nodes. Consider the resonance cone at 1.94 GHz which is shown in Fig. 7. The cone angle at this frequency is 63° and the resonance cone terminates at node 15 along the top edge. For counter-flowing currents to exist, we would expect to find the S_{21} response at nodes 14 and 15 to be similar in magnitude and out-of-phase. Fig. 9 shows the S_{21} magnitude and phase responses measured at nodes 14 and 15. The magnitude response shows that the S_{21} magnitudes for node 14 and node 15 are indeed similar at 1.94 GHz. Thus, the double-peak shown by the magnitude response curve of node 15 is simply the result of counter-flowing streams of current running along either side of the resonance cone core, with the first peak corresponding to a resonance cone angle of 59° and the second peak corresponding to the return current of the resonance cone at an angle of 63°. To wrap up the present discussion, we note from the phase response plot that the two nodes differ in phase by 133° at 1.94 GHz, a phase difference comparable to the simulated results given in [11]. In other words, current flow is approximately out-of-phase across the resonance cone.

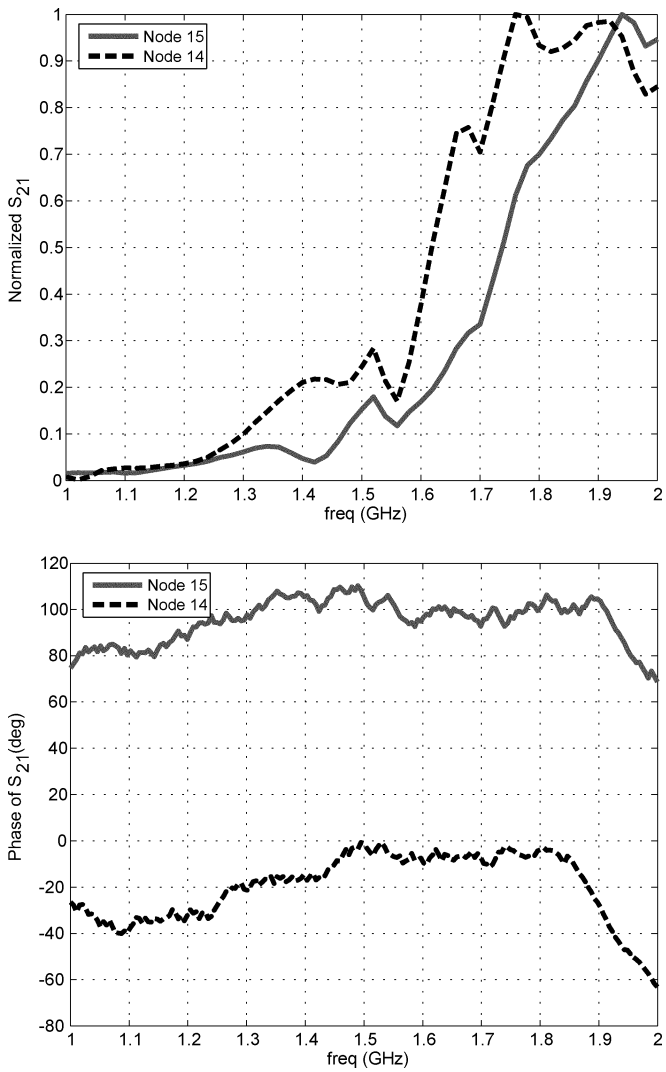

Fig. 9. Normalized forward transmission magnitude and phase responses measured at node 14 and node 15 which confirm experimentally the notion of counter-flowing currents across the resonance cone.

VIII. Conclusion

A quasi-TEM-based theory to describe fields in planar anisotropic transmission-line metamaterials has been presented. It was found that the planar anisotropic transmission-line metamaterial is magnetically anisotropic and the dispersion characteristic becomes hyperbolic when two of the three diagonal elements of the permeability tensor are opposite in sign. Furthermore, analysis by consideration of an infinite electric line current source shows that resonance cone formation is due to the singularity created by the open-branch of the lossless dispersion equation. This conclusion is consistent with the circuit theory analogy presented in [4]. In spite of the electromagnetic interpretation of the resonance cone phenomena presented here, the circuit theory point of view provides an intuitive understanding and a valid approximation to resonance cone formation. Since in circuit theory all interconnect dimensions are regarded as having zero length and all lumped components are regarded as being infinitesimal, therefore in the present context, resonance cones can be viewed, in simplified terms, as the directions of the point-to-point zeros in reactance across the grid surface [4].

Simulation results demonstrate TEM type propagation within the unit cells of the metamaterial which confirms the validity of the quasi-TEM approximation. Resonance cone angle measurements were performed and agreed with the simulations as well as the analytical calculation of the resonance cone angle. Finally, to the authors' best knowledge, experimental verification of counter-flowing currents across the resonance cone is presented for the first time.

Although the quasi-TEM-based theory is limited to structures with a ground plane, it provides a basis for device application

designs. In that context, the resonance cone angle enables us to examine the allowed directions of energy transport as a function of frequency and material parameters. In a more general scenario, measurement of resonance cone angle can also be used as a diagnostic measure to determine the material parameters of the metamaterial.

REFERENCES

[1] K. G. Balmain, A. A. E. Lüttgen, and P. C. Kremer, "Power flow for resonance cone phenomena in planar anisotropic metamaterials," *IEEE Trans. Antennas Propag.*, vol. 51, no. 10, pp. 2612–2618, Oct. 2003.

[2] R. K. Fisher and R. W. Gould, "Resonance cones in the field pattern of a short antenna in an anisotropic plasma," *Phys. Rev. Lett.*, vol. 22, no. 21, pp. 1093–1095, May 1969.

[3] K. G. Balmain and G. A. Oksiutik, "RF probe admittance in the ionosphere: theory and experiment," in *Plasma Waves in Space and in the Laboratory*. Edinburgh, U.K.: Edinburgh Uni. Press, 1969, vol. 1, pp. 247–261.

[4] K. G. Balmain, A. A. E. Lüttgen, and P. C. Kremer, "Resonance cone formation, reflection, refraction, and focusing in a planar anisotropic metamaterial," *IEEE Antennas Wireless Propag. Lett.*, vol. 1, no. 7, pp. 146–149, 2002.

[5] K. G. Balmain, "The impedance of a short dipole antenna in a magnetoplasma," *IEEE Trans. Antennas Propag.*, vol. 12, no. 5, pp. 605–617, Sep. 1964.

[6] L. R. Walker, "Magnetostatic modes in ferromagnetic resonance," *Physical Review*, vol. 105, no. 2, pp. 390–399, January 1957.

[7] P. Kabos and V. S. Staĺmachov, *Magnetostatic Waves and Their Applications*. London, U.K.: Chapman & Hall, 1994.

[8] A. K. Iyer, K. G. Balmain, and G. V. Eleftheriades, "Dispersion analysis of resonance cone behaviour in magnetically anisotropic transmissionline metamaterials," in *Proc. IEEE Antennas and Propagation Society Symp.*, June 2004, vol. 3, pp. 3147–3150.

[9] G. V. Eleftheriades and O. F. Siddiqui, "Negative refraction and focusing in hyperbolic transmission-line periodic grids," *IEEE Trans. Microwave Theory Tech.*, vol. 53, no. 1, pp. 396–403, Jan. 2005.

[10] D. M. Pozar, *Microwave Engineering*, 2nd ed. New York: Wiley, 1998.

[11] K. G. Balmain and A. A. E. Lüttgen, "Planar anisotropic resonancecone metamaterials," in *Negative-Refraction Metamaterials: Fundamental Principles and Applications*, G. V. Eleftheriades and K. G. Balmain, Eds. New York/Piscataway, NJ: Wiley-IEEE Press, Jun. 2005, ch. 6, pp. 249–267.

[12] L. B. Felsen, "Radiation from a uniaxially anisotropic plasma half space," *IEEE Trans. Antennas Propag.*, vol. 11, no. 4, pp. 469–484, Jul. 1963.

[13] P. C. Clemmow, "The theory of electromagnetic waves in a simple anisotropic medium," *Proc. IEE*, vol. 110, no. 1, pp. 101–106, Jan. 1963.

[14] R. F. Harrington, *Time-Harmonic Electromagnetic Fields*. Piscataway, NJ: IEEE Press, 2001.

[15] L. B. Felsen and N. Marcuvitz, *Radiation and Scattering of Waves*. Hoboken, NJ: Wiley, 2003.

[16] L. B. Felsen, "Propagation and diffraction in uniaxially anisotropic regions. i—theory. ii—applications," *Proc. Inst. Elect. Eng.*, vol. 111, no. 3, pp. 445–464, Mar. 1964.

[17] R. K. Fisher and R. W. Gould, "Resonance cones in the field pattern of a radio frequency probe in a warm anisotropic plasma," *Phys. Fluids*, vol. 14, no. 4, pp. 857–867, Apr. 1971.

Joshua K. H. Wong (S'00) received the B.A.Sc. degree in computer engineering from the University of Waterloo, Waterloo, ON, Canada, in 2002. He received the M.A.Sc degree in electrical engineering from the University of Toronto, Toronto, ON, Canada, in 2004 with his thesis on the spatial filtering property in planar anisotropic transmission-line metamaterials.

From 1998 to 2000, he was with the Embedded System Group at Research in Motion (RIM), Waterloo, ON, Canada, where he was engaged in the design and development of non-volatile memory system for mobile handheld devices. From 2000 to 2002, he joined the RF Engineering Group at RIM where he worked on power amplifiers, voltage-controlled oscillators (VCOs) and PLL frequency synthesizers for GSM and CDMA mobile handheld devices. Currently, he is a Ph.D. candidate at The Edward S. Rogers Sr. Department of Electrical and Computer Engineering, University of Toronto. His research interests include adaptive radar cross section (RCS) materials for low-observable vehicles, agile beam steering antennas, thin-film ferro-electric devices and MEMS devices for RF and Microwave applications.

Mr. Wong was a recipient of the 2006 Best Poster Paper Award presented at the IEEE International Workshop on Antenna Technology, held in White Plains, New York, March 6–8, 2006.

Keith G. Balmain (S'56–M'63–SM'85–F'87–LF'97) received the B.A.Sc. degree in engineering physics from the University of Toronto, Toronto, ON, Canada, in 1957. He received the M.S. and Ph.D. degrees in electrical engineering from the University of Illinois, Urbana, in 1959 and 1963, with theses on printed-circuit dipole antennas and spacecraft-borne dipole antennas in anisotropic plasma.

He was an Assistant Professor of electrical engineering at the University of Illinois until 1966. He then joined what is now The Edward S. Rogers Sr. Department of Electrical and Computer Engineering, University of Toronto, where he is a Professor Emeritus. From 1991 to 2001, he was the Senior Chairholder of the NSERC/Bell Canada/Nortel Industrial Research Chair in Electromagnetics. He chaired the Division of Engineering Science for two and a half years until 1987, after which, for a three-year term, he chaired the University of Toronto's Research Board. Currently he leads the Novel Microwave Technologies Thrust within the University of Toronto's Emerging Communications Technology Institute. His research has included antennas in plasma, broadband antennas, electromagnetic compatibility, human electrostatic discharge, radio wave scattering from power lines and buildings, Space Shuttle EMC prediction, electrostatic charging and discharging in spacecraft dielectrics, and microwave metamaterials. He co-authored the second edition of *Electromagnetic Waves and Radiating Systems* (Englewood Cliffs, NJ: Prentice-Hall, 1968).

Dr. Balmain is a Life Fellow of the IEEE "for contributions to the understanding of log-periodic antennas and antennas in plasmas." He was the co-recipient of the IEEE Antennas and Propagation Society (AP-S) 1970 Best Paper Award, and was a co-recipient of a 1992 NASA Group Achievement Award for an "exceptional engineering assessment of plasma effects from electrical grounding for the Space Station Freedom program." He was a member of AP-S AdCom (1974–77), an Associate Editor of *Radio Science* (1978–1980), chair of the Technical Program Committee for the Quebec City 1980 IEEE AP-S International Symposium, and chair of the local Organizing Committee for the Toronto 1999 General Assembly of the International Union of Radio Science (URSI).

George V. Eleftheriades (S'86–M'88–SM'02–F'06) received the diploma (with distinction) from the National Technical University of Athens, Greece, in 1988 and the M.S.E.E. and Ph.D. degrees from the University of Michigan, Ann Arbor, in 1993 and 1989, respectively, all in electrical engineering. He received a diploma (with distinction) in electrical engineering from the National Technical University of Athens, Greece in 1988.

During 1994–1997, he was with the Swiss Federal Institute of Technology, Lausanne, where he developed millimeter- and sub-millimeter-wave receiver technology for the European Space Agency and fast computer-aided design tools for planar packaged microwave circuits. In 1997, he joined the Department of Electrical and Computer Engineering, University of Toronto, Toronto, ON, Canada, where he is now a Professor and a Canada Research Chair (tier 1). He is leading a group of 15 graduate students in the areas of negative-refraction metamaterials and their microwave applications, integrated antennas and components for broadband wireless telecommunications, novel antenna beam-steering techniques, low-loss silicon micromachined components, sub-millimeter-wave radiometric receivers, and electromagnetic design for high-speed digital circuits. He coedited/coauthored a book *Negative-Refraction Metamaterials: Fundamental Principles and Applications* (Hoboken/Piscataway, NJ: Wiley & IEEE Press, 2005).

Prof. Eleftheriades received the Gordon Slemon Award (teaching of design) from the University of Toronto and the Ontario Premier's Research Excellence Award both in 2001. In 2004 he received an E. W. R. Steacie Memorial Fellowship from the Natural Sciences and Engineering Research Council of Canada (this is a national award "to outstanding scientists and engineers who, though still in the early stages of their careers, already enjoy a reputation for original research"). In 2006, he was elected a Fellow of the IEEE "for contributions to conception, analysis and fabrication of electromagnetic materials and their applications." Presently, he serves as an IEEE Distinguished Lecturer for the Antennas and Propagation Society.